J Mater Sci

Metals & corrosion

Microstructural refinement in ultrasonically modified A356 aluminum castings

Katherine E. Rader[1,*], Adrian S. Sabau[2], and Aashish Rohatgi[1]

[1] *Pacific Northwest National Laboratory, P.O. Box 999, Richland, WA 99354, USA*
[2] *Oak Ridge National Laboratory, 1 Bethel Valley Rd, Oak Ridge, TN 37830, USA*

Received: 28 June 2023
Accepted: 29 September 2023

ABSTRACT

Two A356 aluminum alloys (Al–Si–Mg), one with 0.09 wt.% Fe and one with 0.91 wt.% Fe, were cast in a graphite mold with simultaneous local ultrasonic processing to refine the as-cast microstructure. Ultrasonication during casting transformed the morphology of primary Al grains from dendritic (~ 140–290 microns in size) to globular (~ 33–36 microns in size). The alloy with high Fe exhibited globular grains at distances up to 45 mm away from the ultrasound probe, while the alloy with low Fe exhibited globular grains at distances only up to 6 mm away from the ultrasound probe. Near the location of the ultrasound probe (< 2 mm away), a second non-dendritic microstructural morphology was observed with fine aluminum grains (~ 9–25 microns in size). This unique fine-grained morphology has not been previously reported, contains a greater area fraction of Si relative to the globular microstructure, and may be a large, fully eutectic region. Ultrasonication during casting also transformed the morphology of the β-Al$_5$FeSi phase particles (which are deleterious to the strength and ductility of the alloy) in the high Fe alloy from needle-like to rectangular, which could enable the greater use of secondary Al alloys. Thermodynamic simulations conducted to calculate the solidification paths of the two alloys studied predict that the β-Al$_5$FeSi phase begins to form earlier in the alloy with high Fe. Data suggest that the β-Al$_5$FeSi phase (which is more abundant in alloys with high Fe content) may enhance ultrasonically-induced grain refinement.

Introduction

Currently, aluminum (Al) castings account for 60 to 70% of the aluminum used in vehicles [1]. The microstructures of cast aluminum alloys are typically dendritic, inherently less homogeneous, and contain porosity defects. Consequently, they typically have poor mechanical properties, especially compared to wrought materials. Some enhancement in as-cast properties can be achieved by refining the microstructure. One method of refining the microstructure is the use of high thermal conductivity molds (*e.g.*, permanent

---

Handling Editor: P. Nash.

Address correspondence to E-mail: Katherine.Rader@pnnl.gov

https://doi.org/10.1007/s10853-023-08999-y

molds) and/or chills, which increase the local cooling rate during casting [2]. However, chills may not always be practical for certain mold designs and the cooling rate may not necessarily be high enough for refinement further away from the chill. Another method is the addition of grain refiners, which enhance the nucleation rate in the melt [3–5]. However, grain refiners are limited in their ability to efficiently produce grain sizes smaller than ~ 100 microns [4, 5]. Additionally, their grain refining effectiveness decreases with repeated recycling because of a combination of loss of the refiners in the dross and agglomeration of particles [5]. The addition of grain refiners to the melt also changes the overall composition of the alloy, making it more difficult to recycle. Another microstructural refinement method is friction stir processing, which is capable of producing grain sizes less than 100 microns in cast aluminum alloys [6, 7]. However, this technology requires additional processing steps following casting, which can increase the total costs.

Ultrasonic melt processing of molten Al alloys is a casting technique used for purposes such as degassing, fine filtration, and the production of non-dendritic, refined microstructures [8]. The mechanisms for how these unique microstructures are formed can be classified into two categories: those that relate to nucleation and those that relate to the fracture of dendrites. The mechanisms that relate to nucleation put forward that ultrasonic cavitation enhances both homogeneous and heterogeneous nucleation, thus increasing the number of primary Al grains in a given volume of material and thereby decreasing average grain size [8–12]. One proposed mechanism is that collapsing ultrasonic cavities increase undercooling in the melt, promoting *homogeneous* nucleation for primary Al grains [8]. Another proposed mechanism is that ultrasonication increases the wettability of small impurities in the melt, increasing the number of potential *heterogeneous* nucleation sites [9–12]. These mechanisms tend to dominate when ultrasound is applied to the alloy at temperatures above the liquidus. On the other hand, the mechanisms that relate to the fracture of dendrites put forward that a combination of local remelting at the root of dendrite arms along with mechanical deformation leads to the fracture of dendrites, resulting in smaller-sized grain units [13–15]. This mechanical deformation may come from the implosion of ultrasound cavitation bubbles, the movement of clouds of ultrasound cavitation bubbles, and/or acoustic flow [13–15]. These mechanisms are only relevant when ultrasound is applied to semi-solid alloy (*i.e.*, at temperatures below the liquidus). Recent *in-situ* radiography experiments have observed the growth, movement, and collapse of ultrasound bubbles in molten Al-Cu alloys and have also observed the fracture of aluminum dendrites in a *solidifying* Al-Cu alloy [15–20]. The final ultrasonically-refined microstructure has improved strength, ductility, and fatigue life compared to that of the dendritic microstructures [8, 21]. This ultrasonically-induced improvement in strength and ductility has been demonstrated by preliminary results from this study [22].

This study is part of a larger investigation to locally apply ultrasonic processing in an Al casting to refine the local as-cast microstructure. Rather than applying ultrasound to molten aluminum before/during pouring, in this work ultrasound is applied to the Al as it solidifies in a permanent mold. This approach allows for the active application of the ultrasound field to targeted locations within a larger casting during the casting process itself. This is in comparison to passive chills, bulk grain-refiners, and/or post-casting steps that employ mechanical techniques such as friction processing. In this study, two A356 Al alloys were used, one with low Fe content and another one with added Fe content. The purpose of studying an alloy with added Fe content is to determine if ultrasound can also refine the microstructure of secondary alloys, thus enabling more widespread use of them. Both alloys were cast in a graphite mold. Ultrasound was applied via a probe inserted into the mold through the mold wall. The resultant microstructures were characterized using optical microscopy, scanning electron microscopy, and electron backscatter diffraction (EBSD). Thermodynamic simulations were conducted to gain insight on the phase types and amounts for the two alloys studied.

Methods and materials

Materials

This study investigated two Al–Si–Mg alloys provided by Eck Industries, Inc. Table 1 lists the composition of each alloy. The first alloy is an A356 Al alloy with 0.09 wt.% Fe. The second alloy is an A356 Al alloy produced with additional Fe content (A356 + Fe). This raised the Fe composition of the alloy to 0.91 wt.%, which mimics the “high” Fe content seen in recycled Al alloys [23]. Prior studies of ultrasonic melt

Table 1 Composition, in wt.%, of the two alloys studied

Alloy	Si	Mg	Fe	Ti	Cu	Mn	Ni	Sr	Ga	V	Al
A356	6.72	0.42	0.09	0.11	0.00	0.00	0.01	0.00	0.01	0.02	Bal
A356 + Fe	6.78	0.35	0.91	0.11	0.01	0.01	0.00	0.01	0.00	0.02	Bal

processing of 356 alloys have not investigated an alloy with Fe amounts this high [8, 9, 15, 19, 21]. Both alloys also contain less than 0.002 wt.% Zr and less than 0.001 wt.% Cr, Zn, and Co. The A356 + Fe alloy also contains 0.003 wt.% B.

Casting

For casting experiments, approximately 200 g of Al was melted in an alumina crucible inside of a box furnace, heated to approximately 720 °C, and cast in a cylindrical graphite mold at room temperature. Graphite was chosen as the mold material because casting Al in a graphite mold at room temperature can simulate the solidification rates of permanent mold casting techniques, which typically use a preheated steel mold [24]. The inner diameter of the mold was 45 mm and the walls were 8 mm thick. Ultrasound was applied using a Sonics VCX 750 ultrasonic liquid processor with a CV-33 ultrasonic converter and a 630–0220 (13 mm dia.) cylindrical ultrasonic probe with a 127 mm extender. The tip of the ultrasound probe, which was made of Ti-6Al-4V, was inserted into the mold through the mold wall, regardless of whether or not ultrasound was applied, see Fig. 1. The probe was inserted into the mold prior to pouring the molten Al and was removed once the Al fully solidified and cooled. To minimize exposure between the liquid Al and the Ti-6Al-4V probe, the tip of the probe only protruded a few mm into the mold from the mold wall and was coated with boron nitride lubricant. Thermocouples were placed on the probe outside of the mold to monitor the temperature of the probe. A type-K thermocouple was placed in the mold in front of the face of the ultrasound probe to measure the temperature of the Al as it cooled. Temperature data were recorded at a rate of 1 Hz.

For the experiments where ultrasound was applied, ultrasound was started just before the molten Al alloy was poured into the mold and was stopped once the temperature of the Al cooled below the solidus. The ultrasound probe oscillated longitudinally at a frequency of 20 kHz and power varied up to 750 W to maintain a set peak-to-peak amplitude of 33 µm (though for select experiments, the amplitude setting was raised to 78 µm). (Note: the actual peak-to-peak amplitude was likely smaller than the set amplitude as the temperature at the tip of the probe was hotter than room temperature). Both the ultrasonic converter and the mold were clamped in place to ensure that the probe remained in contact with the Al throughout solidification. After casting, select specimens were heat treated to a T6 condition by solution heat treating at 540 °C for 6 h, quenching in hot water, then aging at 155 °C for 4 h [25].

Microstructural characterization

Optical microscopy (OM) and scanning electron microscopy (SEM) were used to characterize the microstructures and measure secondary dendrite arm spacing. Castings were sectioned along the

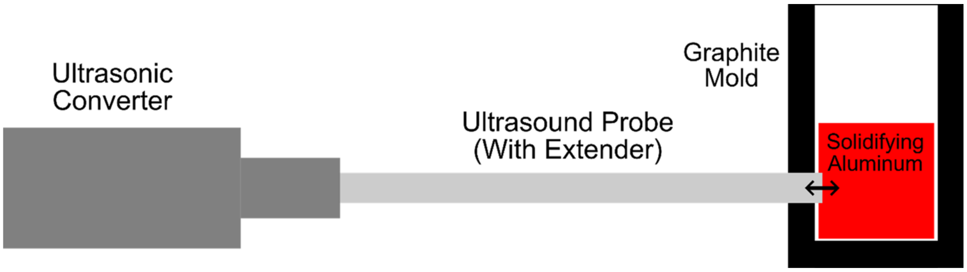

Figure 1 Schematic depicting the ultrasound probe (with a 127 mm extender) inserted into the graphite mold via a hole in the mold wall. The probe oscillated longitudinally to ultrasonically process the Al as it solidified in the mold.

longitudinal axis of the ultrasound probe to produce optical microscopy specimens. These specimens were polished and etched using Keller's reagent to reveal phases for OM and were then repolished for SEM. A JOEL JSM-7001F Schottky Emission SEM was used. Primary Al grains were identified and imaged using a Bruker Quantax e-Flash HR electron backscatter diffraction (EBSD) detector. Misorientation angles of 15° or more were defined as high-angle grain boundaries separating grains. Only grains with at least 25 pixels were counted and regions of less than 10 unindexed pixels were absorbed into the surrounding grain. Iron-rich β-Al_5FeSi particles and eutectic silicon particles were identified using a Bruker Quantax X-Flash|60 energy dispersive X-ray spectroscopy (EDS) detector and imaged in backscatter diffraction mode. ImageJ software was used to measure the equivalent grain diameter, sphericity, and aspect ratio of the Al dendrites/grains, Si particles, and β phase particles [26]. Equivalent grain diameter, *i.e.*, the diameter of the dendrite/grain if it were a perfect circle, is defined as $\sqrt{(4A/\pi)}$, where A is the area of the grain. Sphericity, sometimes referred to as roundness, is defined as $4\pi AP^{-2}$, where P is the perimeter of the grain/particle. Sphericity values range from 0 to 1, with values closer to 1 indicating a more circular morphology and values closer to 0 indicating a more needle-like morphology. Aspect ratio is defined as the major axis of the ellipse fit to the grain/particle divided by the minor axis of the ellipse fit to the grain/particle. ImageJ software was also used to quantify area fraction of phases, which for subsequent discussion is assumed to be equivalent to volume fraction. All measurement uncertainties listed in this study are the sample estimate of standard deviation unless otherwise specified.

Thermodynamic simulations

Thermodynamic simulations were conducted for solidification of the two alloys considered in this study. Experimental temperature data from several casting experiments were used to estimate the cooling rate during casting. The subsequent heat treatments were not simulated. Thus, microstructure data are presented only to highlight the different phases and their amounts between the two alloys considered without an assessment of model accuracy. The microstructure model in ProCAST, which is based on the CompuTherm software with the Pandat databases, was used to conduct the thermodynamic simulations for the two alloys considered based on a back diffusion (BD) model for a constant cooling rate of 1.37 °C/s (calculated from experimental temperature data just below the solidus) and a Scheil model. The Scheil model was included for comparison. The terminology from the ProCAST/CompuTherm simulations is used in sections discussing the simulation work [27, 28].

Results

Casting

Figure 2 shows an example of thermocouple temperature data acquired during the solidification of the A356 alloy with the application of local ultrasonic processing. The liquidus, solidus, and binary Al-Si eutectic temperatures are indicated in the figure, as well as the superheat temperature of the molten Al. Aside from the main Al-Si eutectic phase transformation at ~ 573 °C, the A356 alloy exhibits another eutectic reaction near the end of solidification, at less than 5% liquid fraction [29]. Since the application of ultrasound is sought at much larger liquid fractions than that of the ternary eutectic, all references made in in the remainder of this study to the eutectic phase transformation refers to the main Al-Si eutectic transformation at ~ 573 °C. Two average cooling rates are observed, one between the liquidus and the eutectic temperature, and one between the eutectic temperature and

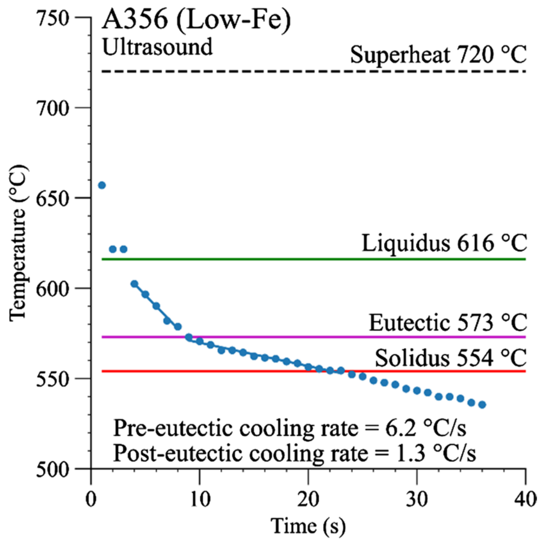

Figure 2 Experimentally measured temperature evolution for the A356 alloy cast with local ultrasonic processing.

the solidus (*i.e.*, the temperature at which the total solid fraction is 100%). These average cooling rates are defined as the pre-eutectic cooling rate and the post-eutectic cooling rate, respectively. Among multiple casting experiments, the average pre-eutectic cooling rate was 5.4 ± 1.0 °C/s and the average post-eutectic cooling rate was 1.4 ± 0.5 °C/s. Both the pre-eutectic and post-eutectic cooling rates were relatively insensitive to the presence/absence of local ultrasonic processing and the Fe content of the alloy. The average cooling rate across casting experiments in this work is similar to the cooling rates typically observed in permanent mold casting processes, which typically range from 0.1 to 1 °C/s [24].

Microstructural characterization

Alloys that were cast without local ultrasonic processing (*i.e.,* the A356 and A356 + Fe control castings) exhibited only a dendritic morphology, as shown in Fig. 3. The specimens were etched so that Al appears lighter and Si appears darker. The mean secondary dendrite arm spacing (SDAS) of the primary Al dendrites, measured at multiple locations in both castings, is 24 ± 5 μm for the A356 control casting and 23 ± 5 μm for the A356 + Fe control casting.

Alloys that were cast with local ultrasonic processing (*i.e.,* the A356 and A356 + Fe ultrasonicated castings) exhibited regions with three distinct microstructural morphologies: globular grains, fine grains, and dendritic grains, as shown in Figs. 4 and 5. For the A356 ultrasonicated casting, the two non-dendritic morphologies were observed only within 6 mm of the ultrasound probe, while the dendritic morphologies were observed at greater distances (> 6 mm) away from the ultrasound probe. For the A356 + Fe ultrasonicated casting, the globular grains were observed at further distances, up to 45 mm away from the ultrasound probe, and the dendritic grains were only observed near the mold wall. Stitched optical micrographs that show the regions of the three distinct morphologies relative to the ultrasound probe are provided in Appendix A.

Since both of the control castings exhibited only dendritic morphology, the presence of dendrites in the ultrasonicated castings indicates that only a selected region in the ultrasonicated castings was modified while the remainder of the casting retained a dendritic morphology. Therefore, the boundary between the non-dendritic and dendritic morphologies in the ultrasonicated castings indicates the boundary separating the ultrasonically modified and unmodified zones of the casting, respectively. The total area of the ultrasonically modified zones in the A356 and A356 + Fe ultrasonicated castings is 60 mm^2 and 1230 mm^2, respectively. Increasing the peak-to-peak vibrational amplitude setting of the ultrasound probe from 33 μm to 78 μm did not increase the size of the ultrasonically-modified zone in the A356 ultrasonicated casting (see Appendix A). However, the temperature of the probe when the vibration amplitude was set at 78 μm was hotter than the temperature of the probe during other casting experiments. Therefore, it is possible that the actual vibrational

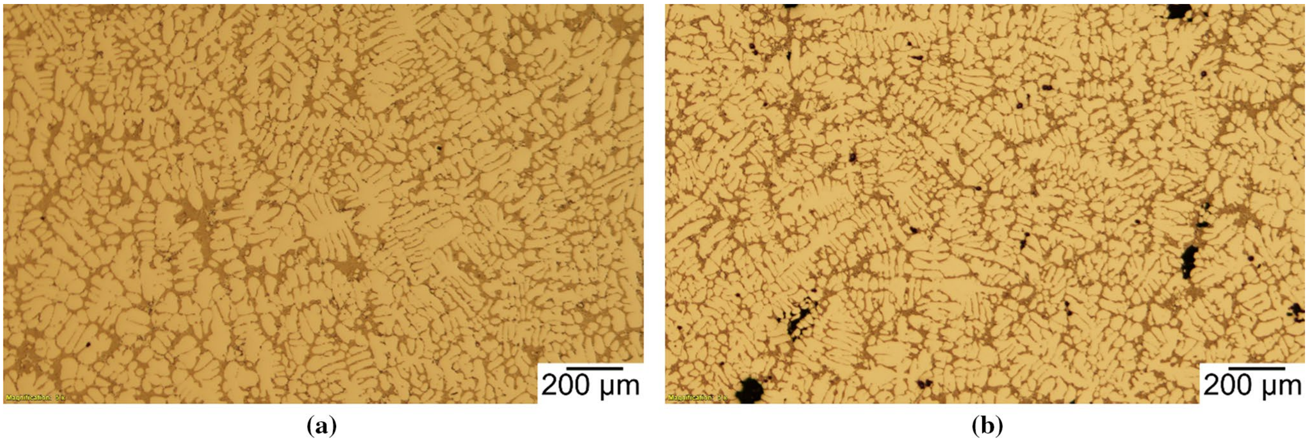

Figure 3 Optical micrographs of dendritic microstructures representative of the microstructure observed in the **a** A356 control casting and **b** A356 + Fe control casting.

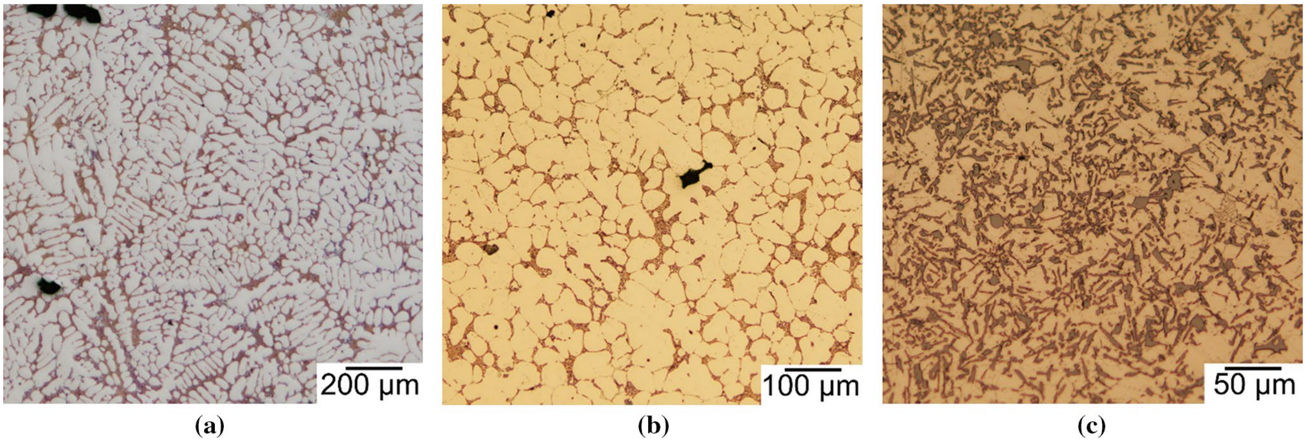

Figure 4 Optical micrographs of the **a** dendritic microstructure, **b** globular microstructure, and **c** fine-grained microstructure representative of the three different microstructure morphologies observed in the A356 ultrasonicated casting.

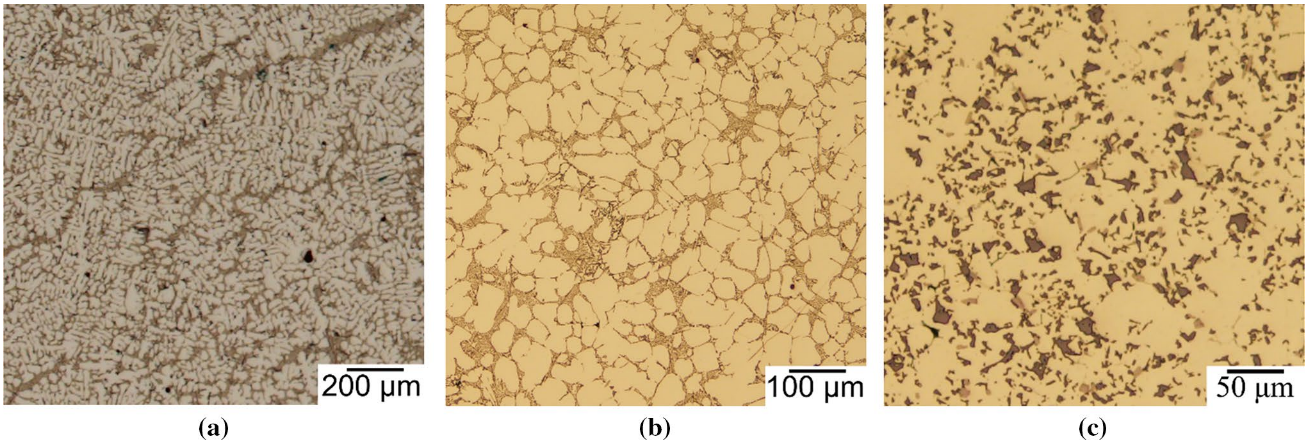

Figure 5 Optical micrographs of the **a** dendritic microstructure, **b** globular microstructure, and **c** fine-grained microstructure representative of the three different microstructure morphologies observed in the A356 + Fe ultrasonicated casting.

amplitude did not change much relative to when the amplitude was set at 33 mm.

Primary aluminum dendrites/grains

Electron backscatter diffraction (EBSD) was used to quantify the size and shape of the primary Al grains. Figure 6 presents inverse pole figure maps (IPF-Z) of the dendritic microstructure of the A356 control casting and the non-dendritic microstructures of the A356 ultrasonicated casting. The IPF-Z maps were captured in the vicinity of the regions depicted in optical micrographs in Figs. 3a, 4b, and 4c. The mean equivalent grain diameter of the primary Al dendrites in the A356 control casting is 290 ± 320 (with an area-weighted mean diameter is 830 μm). In comparison, the mean equivalent grain diameter of the primary Al globular grains and fine-grains in the A356 control casting are 33 ± 20 μm and 25 ± 16 μm, respectively (with area-weighted mean diameters are 58 μm and 46 μm, respectively). Both of these mean equivalent grain diameters are similar to the mean SDAS of the A356 control casting (24 ± 5 μm). While the Al grains in the fine-grained microstructural morphology are only 24% smaller, on average, than those in the globular microstructural morphology, the fine-grained morphology is distinct from the globular microstructure due to the greater

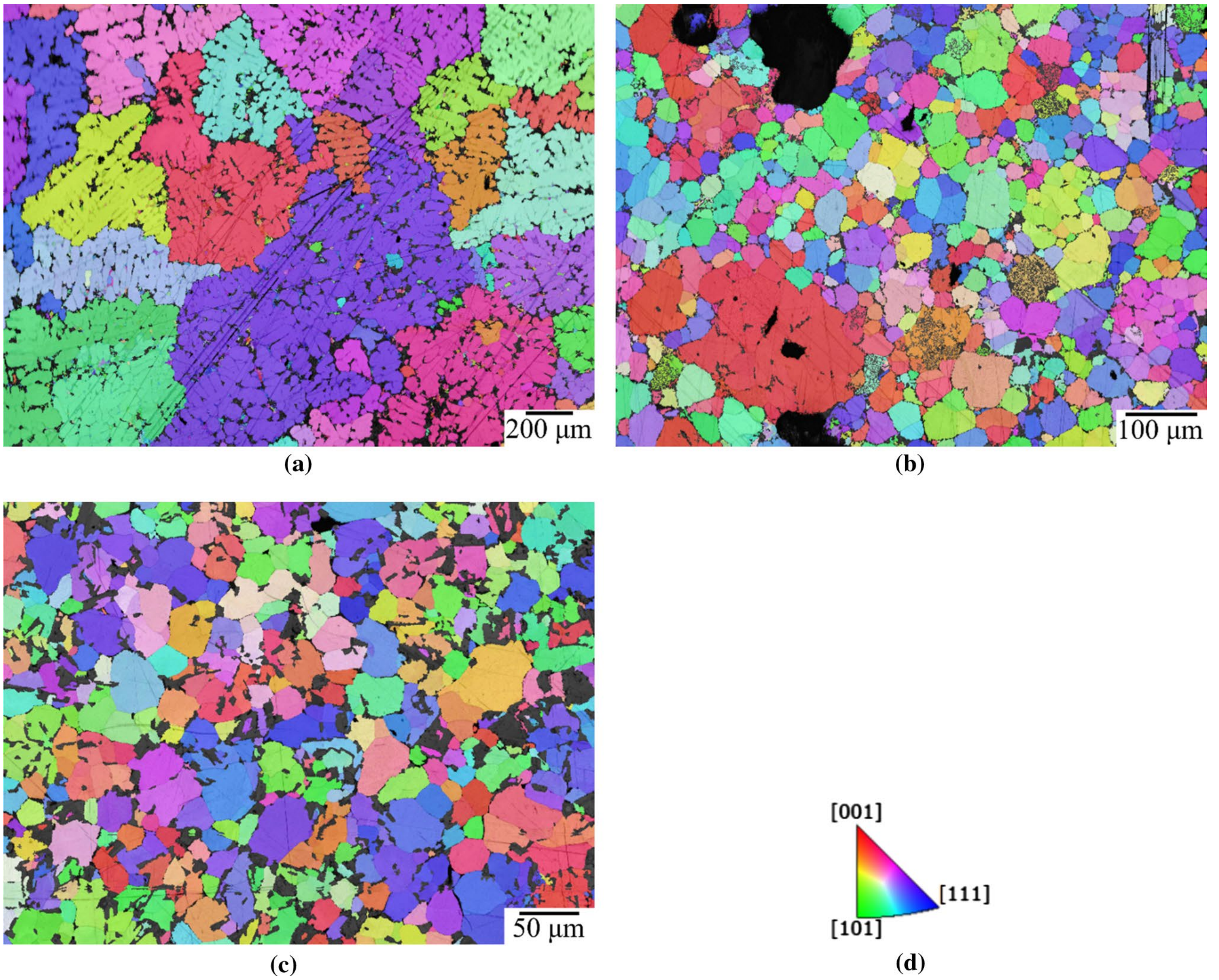

Figure 6 Inverse pole figure (IPF-Z) maps of **a** the dendritic microstructure of the A356 control casting and of **b** the globular microstructure and **c** fine-grained microstructure of the A356 ultrasonicated casting. Only Al grains are indexed. The crystallographic orientation of each Al grain relative to the incident electron beam (*z*-axis) can be identified using the color key **d** in the online version of the article.

area fraction of Si phase particles in the fine-grained region, ~ 15% compared to ~ 6% (see Fig. 4b and 4c).

Figure 7 presents inverse pole figure maps (IPF-Z) of the dendritic microstructure of the A356 + Fe control casting and the non-dendritic microstructures of the A356 + Fe ultrasonicated casting. The IPF-Z maps were captured in the vicinity of the regions depicted in optical micrographs in Fig. 3b, 5b, and 5c. Some of the grain size data for the A356 + Fe ultrasonicated casting were presented as part of preliminary results from this study in Ref. [22]. The mean equivalent grain diameter of the primary Al dendrites is 140 ± 210 µm (with an area-weighted mean diameter is 1400 µm). The mean equivalent grain diameter of the primary Al grains in the globular microstructure and fine-grained microstructure are 36 ± 27 µm (with an area-weighted mean diameter is 86 µm), which is similar to the mean SDAS of the A356 + Fe control casting (23 ± 5 µm). The mean equivalent grain diameter of the Al grains is 9.3 ± 5.3 µm (with an area-weighted mean diameter is 16 µm), which is 74% finer than the globular grains.

Table 2 summarizes the mean equivalent grain diameter, sphericity, and aspect ratio of the primary Al grains in each microstructural morphology region for both of the alloys studied. In the A356 alloy, ultrasonication decreased the equivalent

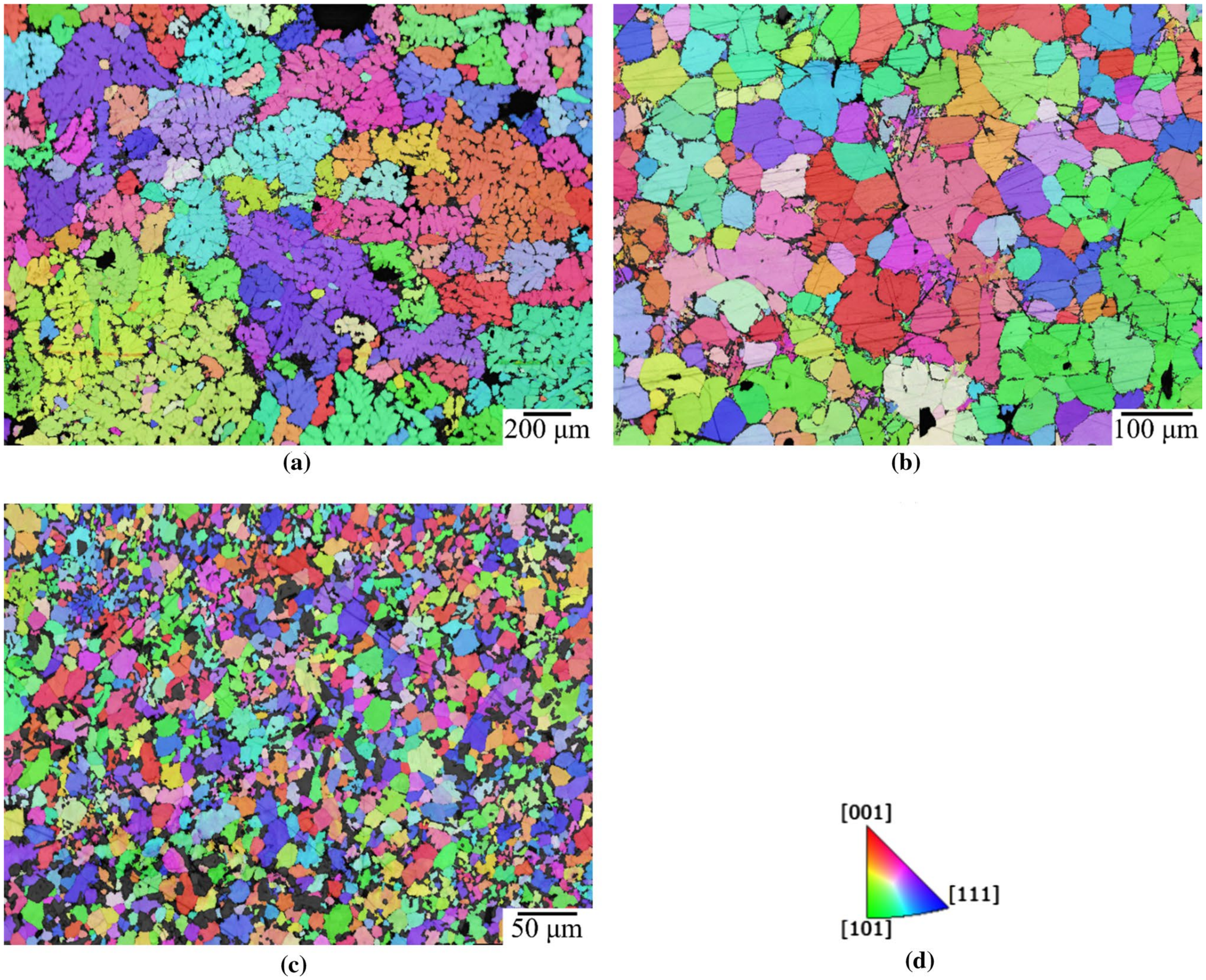

(a)

(b)

(c)

(d)

Figure 7 Inverse pole figure (IPF-Z) maps of **a** the dendritic microstructure of the A356+Fe control casting and of **b** the globular microstructure and **c** fine-grained microstructure of the A356+Fe ultrasonicated casting. Only Al grains are indexed. The crystallographic orientation of each Al grain relative to the incident electron beam (*z*-axis) can be identified using the color key **d** in the online version of the article.

Table 2 Summary of mean equivalent grain diameter, mean sphericity, and mean aspect ratio of primary Al grains by alloy and microstructure regions

Alloy	Microstructure	Eq. Grain Dia. (μm)	Sphericity	Aspect Ratio
A356	Dendritic (control casting)	290 ± 320	0.36 ± 0.25	2.1 ± 1.0
	Globular	33 ± 20	0.52 ± 0.15	1.5 ± 0.4
	Fine-grained	25 ± 16	0.46 ± 0.18	1.7 ± 0.6
A356 + Fe	Dendritic (control casting)	140 ± 210	0.39 ± 0.22	1.8 ± 0.2
	Globular	36 ± 27	0.48 ± 0.18	1.5 ± 0.4
	Fine-grained	9.3 ± 5.3	0.56 ± 0.17	1.8 ± 0.6

grain diameter of the Al grains by 89% and 91% in the globular and fine-grained regions, respectively, compared to the Al dendrites in the control casting (290 μm). In the A356 + Fe alloy, ultrasonication decreased the equivalent grain diameter of the Al grains by 74% and 93% in the globular and fine-grained microstructural morphologies, respectively, compared to the Al dendrites in the control casting (140 µm). For both the A356 and A356 + Fe alloys, ultrasonication increased the sphericity and decreased aspect ratio, suggesting that the primary Al grains of the non-dendritic microstructural morphologies are rounder and more equiaxed than the dendritic grains of the control castings. However, the differences in sphericity and aspect ratio between the different microstructural morphologies are less than the respective measurement uncertainties, and therefore cannot be considered statistically significant.

Si particles

Figure 8 shows the as-cast microstructures of the A356 control and ultrasonicated castings with particular focus on the Si phase particles. The morphology of the Si particles in the dendritic microstructure is fibrous. The Si particles in the globular microstructure have a similar morphology, but are slightly coarser (with 33% larger equivalent grain diameter). On the other hand, the morphology of the Si particles in the fine-grained microstructure is flake-like and highly angular.

Figure 9 shows the microstructures of the A356 castings after the T6 heat treatment

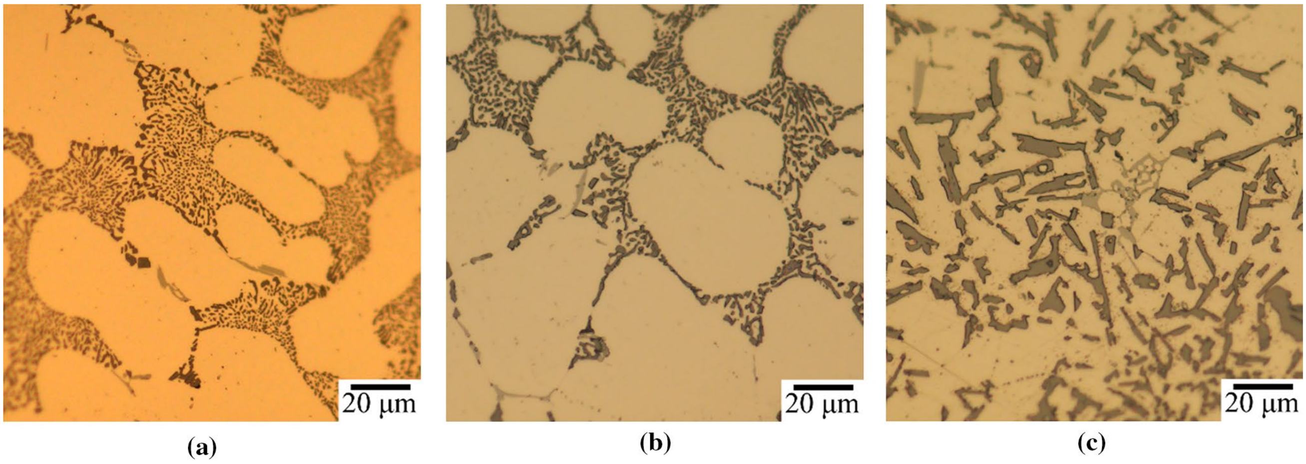

Figure 8 Optical micrographs depicting the morphology of the Si phase particles (dark brown in color) in the as-cast conditions of: **a** the dendritic region of A356 control casting, **b** the globular region of A356 ultrasonicated casting, and **c** the fine-grained region of A356 ultrasonicated casting.

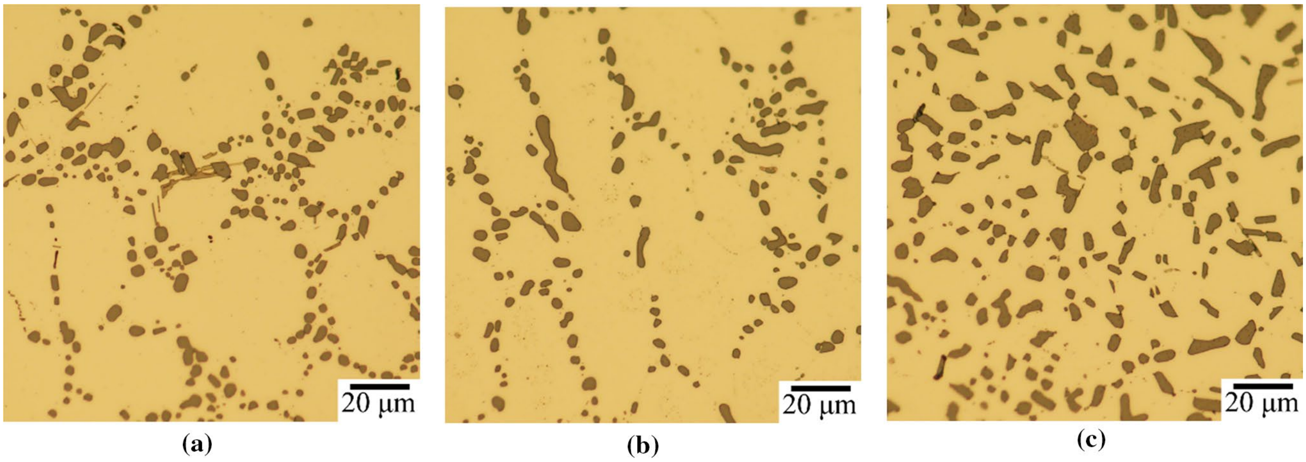

Figure 9 Optical micrographs depicting the morphology of the Si phase particles (dark brown in color) in the T6 condition for: **a** the dendritic region of A356 control casting, **b** the globular region of A356 ultrasonicated casting, and **c** the fine-grained region of A356 ultrasonicated casting.

(solutionization + artificial aging). Table 3 lists the area fraction, mean equivalent diameter, and sphericity of the Si particles in the T6 condition. In all three microstructures, the mean equivalent diameter and sphericity of the Si phase particles increased relative to the as-cast condition and the aspect ratio decreased indicating that the T6 heat treatment caused the Si particles to become rounder and more equiaxed. Compared to the Si particles of the dendritic microstructure, the Si particles of the globular microstructure are smaller (with 12% smaller equivalent diameter) and rounder (with 32% greater sphericity), on average, while the Si particles of the fine-grained microstructure are larger (with 31% larger equivalent diameter) but still rounder (with 26% greater sphericity), on average. The smaller and rounder Si particles in the globular microstructure could produce higher ductility levels, and subsequently higher strength levels, compared to the control casting. The area fraction of Si phase particles in the globular microstructure is similar to that of the dendritic (un-sonicated) microstructure, 6.2% and 6.4%, respectively. The region near the probe with a fine-grained microstructure, however, has a greater area fraction of Si phase particles, 14.9%. This area fraction is similar to the volume fraction of Si in the Al-Si eutectic, 14.3% [30], which is slightly higher than the weight fraction of Si in the Al-Si eutectic, 12.6 wt.%.

Figure 10 shows the as-cast microstructures of the A356 + Fe control and ultrasonicated castings with particular focus on the Si phase particles. The Si particles of the dendritic microstructure in the control casting are fine and fibrous in morphology. The Si particles of the globular microstructure have a similar morphology, but are coarser (with 43% greater equivalent diameter). On the other hand, the Si particles of the fine-grained microstructure are irregular and highly angular in shape, and are significantly coarser than the Si particles of the dendritic microstructure (with 159% greater equivalent diameter).

Figure 11 depicts the microstructures of the A356 + Fe castings after the T6 heat treatment. Table 3 lists the area fraction, mean equivalent diameter, and

Table 3 Summary of area fraction, mean equivalent diameter, and sphericity of Si particles in the T6 condition by alloy and microstructure

Alloy	Microstructure	Area Fraction (%)	Eq. Dia. (μm)	Sphericity
A356	Dendritic (control casting)	6.4	4.45 ± 1.08	0.50 ± 0.24
	Globular	6.2	3.90 ± 1.66	0.66 ± 0.25
	Fine-grained	14.9	5.84 ± 2.45	0.63 ± 0.22
A356 + Fe	Dendritic (control casting)	8.2	2.97 ± 1.23	0.47 ± 0.24
	Globular	8.1	3.02 ± 1.35	0.49 ± 0.21
	Fine-grained	16.8	6.02 ± 3.39	0.58 ± 0.22

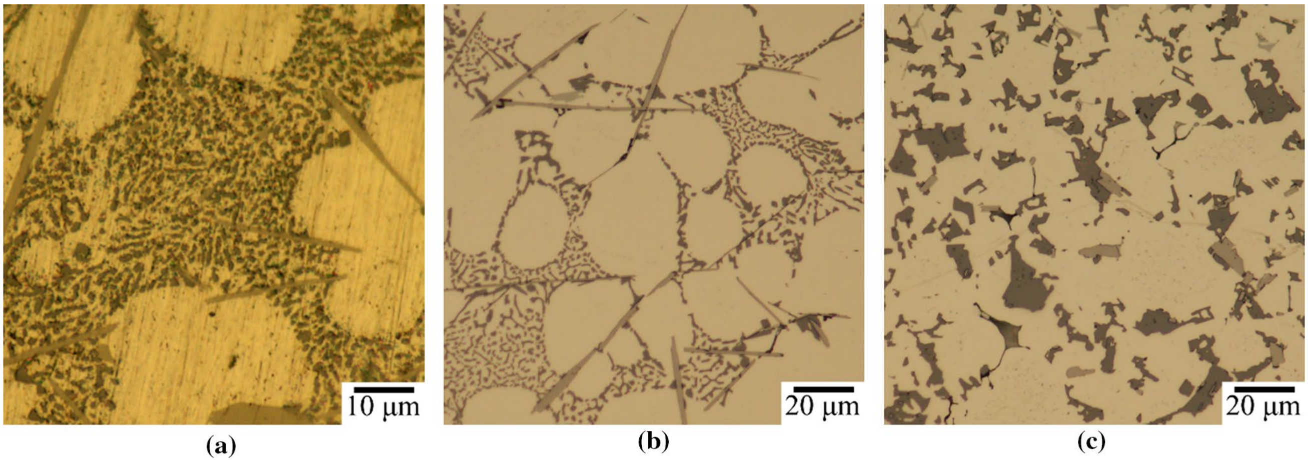

Figure 10 Optical micrographs depicting the morphology of the Si phase particles (dark brown in color) in the as-cast conditions of: **a** the dendritic region of the A356 + Fe control casting, **b** the globular region of the A356 + Fe ultrasonicated casting, and **c** the fine-grained region of the A356 + Fe ultrasonicated casting.

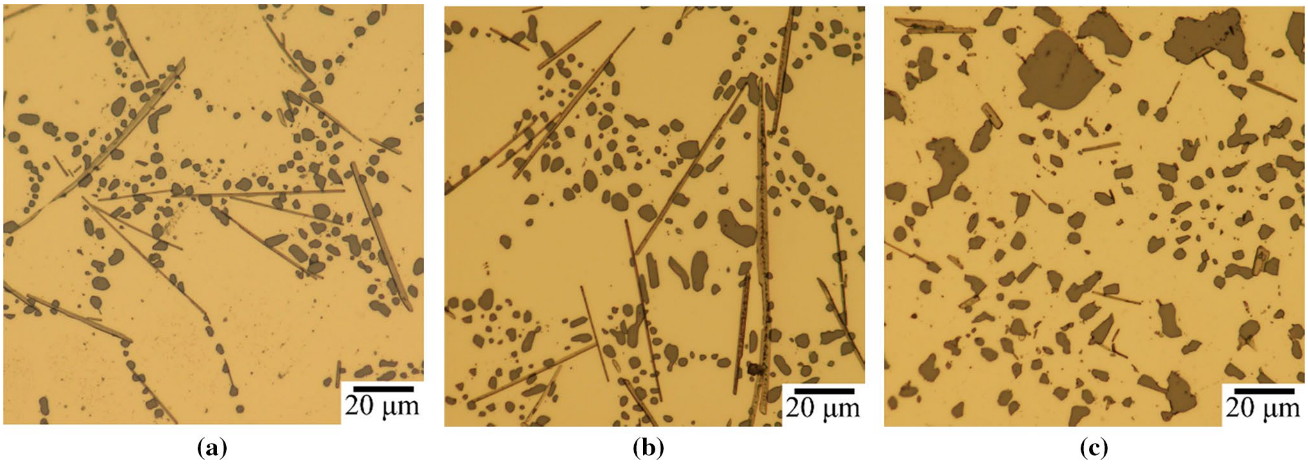

(a) (b) (c)

Figure 11 Optical micrographs depicting the morphology of the Si phase particles (dark brown in color) in the T6 condition for: **a** the dendritic region of the A356 + Fe control casting, **b** the globular region of the A356 + Fe ultrasonicated casting, and **c** the fine-grained region of the A356 + Fe ultrasonicated casting.

sphericity of the Si particles in the T6 condition. As in the A356 castings, the T6 heat treatment increases the average size of the Si phase particles and causes them to become rounder and more equiaxed. The Si particles of the dendritic and globular microstructures are similar in area fraction, equivalent diameter, and sphericity. The Si particles in the fine-grained microstructure near the ultrasound probe, however, are approximately twice as large as those of the dendritic and globular microstructures. As in the A356 castings, the area fraction of Si particles in the fine-grained microstructure, 16.8%, is twice that of the dendritic and globular microstructures in the A356 castings. The large and abundant Si particles in the fine-grained microstructure may provide increased wear resistance analogous to the primary Si particles in hypereutectic Al-Si alloys.

β-Al$_5$FeSi phase particles

In addition to transforming the primary Al grains from dendritic to globular and fine, equiaxed grains, the application of ultrasound also transformed the morphology of the β-Al$_5$FeSi phase particles in the A356 + Fe castings. (The A356 alloy only contained trace amounts the β-Al$_5$FeSi phase and therefore was not considered for this analysis.) Fig. 12 depicts the needle-like β-Al$_5$FeSi phase particles of the A356 + Fe control casting. Figure 13 depicts the β-Al$_5$FeSi phase particles of the A356 + Fe ultrasonicated casting within the globular region, but at different distances from the ultrasound probe. At distances less than 5 mm, the β-Al$_5$FeSi phase particles are rectangular in shape (see Fig. 13a). At distances greater 5 mm, however, the β-Al$_5$FeSi phase particles are needle-like in shape and 10s to 100s of microns in length (see Fig. 13b), similar to their morphology in the A356 + Fe control casting. Figure 14 depicts the β-Al$_5$FeSi phase particles of the A356 + Fe ultrasonicated casting within the fine-grained region, which was observed at distances within 2 mm of the ultrasound probe. The morphology of these particles is rectangular, the same morphology of the particles in the globular region at distances less

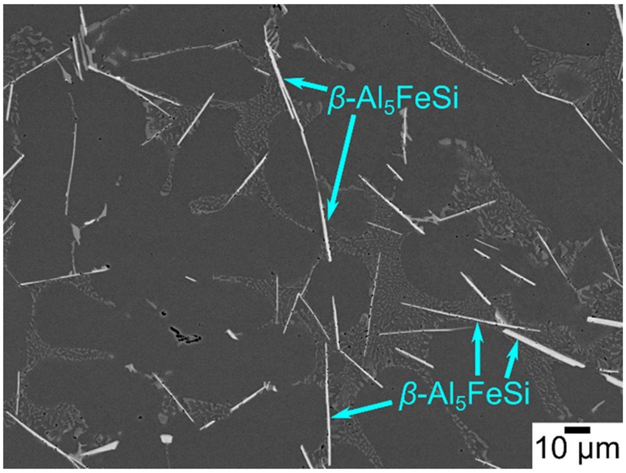

Figure 12 An SEM micrograph, taken in backscatter electron mode, showing the needle-like β-Al$_5$FeSi particles (white), in the dendritic microstructure of the A356 + Fe control casting approximately 15 mm in front of the ultrasound probe.

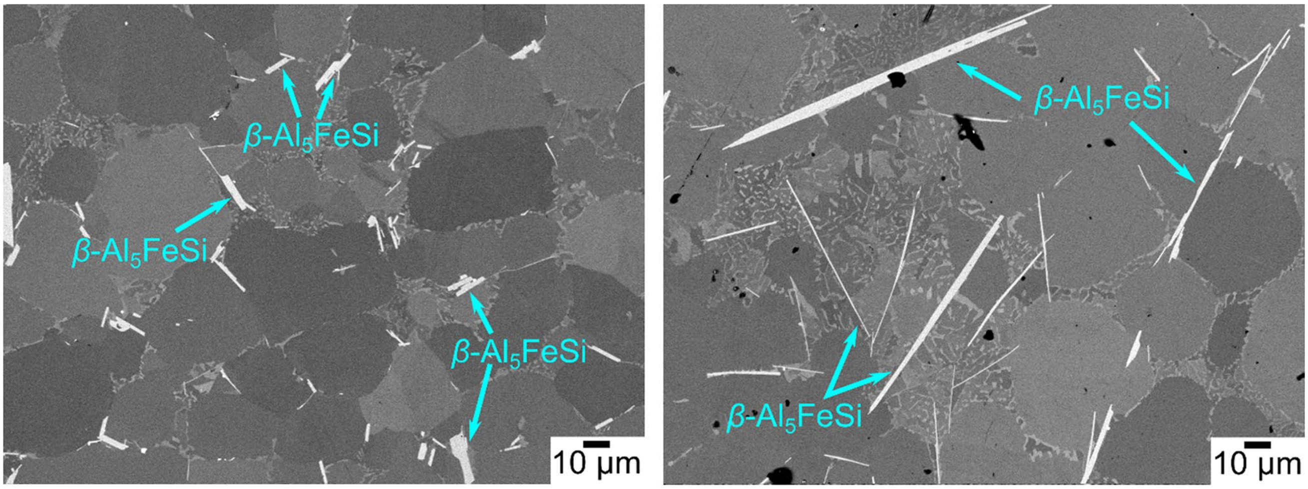

(a) (b)

Figure 13 SEM micrographs, taken in backscatter electron mode, showing the β-Al$_5$FeSi particles (white) in the globular region of the A356 + Fe ultrasonicated casting **a** 2 mm in front of the ultrasound probe and **b** 15 mm in front of the ultrasound probe. The morphology of these β phase particles is rectangular near the ultrasound probe (< 5 mm) and needle-like further away from the ultrasound probe (> 5 mm).

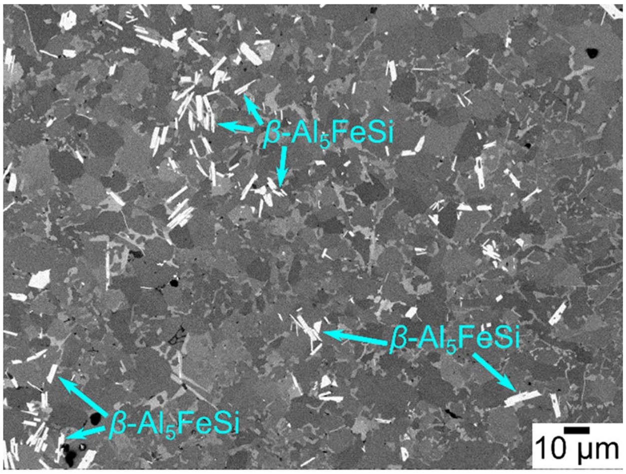

Figure 14 An SEM micrograph, taken in backscatter electron mode, showing the rectangular morphology of β-Al$_5$FeSi particles (white) in the fine-grained region of the A356 + Fe ultrasonicated casting.

than 5 mm from the ultrasound probe. A summary of the mean equivalent diameter, sphericity, and aspect ratio of the β-Al$_5$FeSi phase particles by region and distance from the ultrasound probe is listed in Table 4.

Thermodynamic simulations

Figure 15 shows the weight fraction of each solid phase calculated as the A356 and A356 + Fe alloys cooled through the solidification range using the back diffusion (BD) simulation. For the A356 alloy, the calculated liquidus is 616 °C, the calculated eutectic temperature (*i.e.*, the temperature at which the main binary eutectic reaction occurs and the eutectic Al and eutectic Si phases are expected to come out of the liquid) is 573 °C, and the calculated solidus (*i.e.*, the temperature at which the total solid fraction is 100%) is 554 °C. For the A356 + Fe alloy,

Table 4 Summary of the mean equivalent diameter, sphericity, and aspect ratio of β-Al$_5$FeSi particles in the A356 + Fe castings

Microstructure	Eq. Dia. (µm)	Sphericity	Aspect Ratio
Dendritic (control casting)	3.3 ± 1.7	0.16 ± 0.11	14 ± 11
Globular (< 5 mm from ultrasound probe)	2.5 ± 1.9	0.27 ± 0.18	5.7 ± 3.2
Globular (> 5 mm from ultrasound probe)	2.7 ± 2.2	0.08 ± 0.09	27 ± 32
Fine-grained	2.0 ± 1.6	0.34 ± 0.18	4.2 ± 3.2

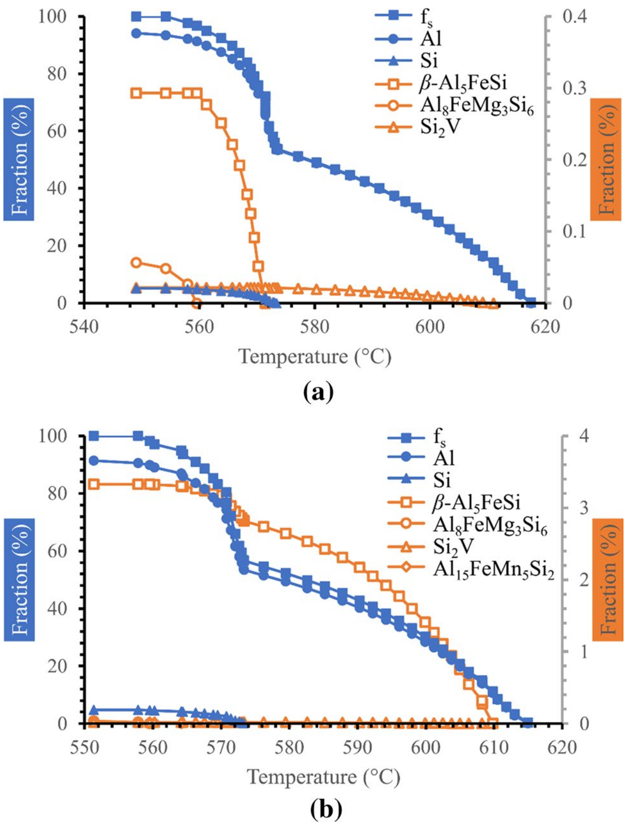

(a)

(b)

Figure 15 Calculated total solid fraction (f_s) and wt.% fraction of each phase using the Al material database CompuTherm and microstructure module in ProCAST for **a** A356 and **b** A356 + Fe alloys using BD model for a constant cooling rate of 1.37 °C/s. Data in solid blue symbols correspond to the left *y*-axis, while the open orange symbols correspond to the right *y*-axis. Note the difference in the scale of right *y*-axes in **a** and **b**.

the calculated liquidus, eutectic, and solidus temperatures are 613 °C, 573 °C and 558 °C, respectively. These predicted temperatures agree with the published typical physical properties of 356.0 [25]. The A356 + Fe alloy is expected to have approximately 11 to 12 times more of the β-Al_5FeSi phase than the A356 alloy. In the A356 + Fe alloy, the β-Al_5FeSi phase is predicted to come out of the liquid at 608 °C, whereas in the A356 alloy it is not expected to form until 571 °C.

Table 5 lists the thermodynamically predicted phases and their amounts at the end of solidification for the A356 and A356 + Fe alloys, using two different models, back diffusion (BD) and Scheil. The primary difference between the predicted phase fractions of the two models is that the Scheil model predicted approximately 0.3% of the Mg_2Si phase in both alloys while the BD model did not predict any Mg_2Si phase. Neither EDS nor EBSD analysis of the metallography specimens was able to detect any Mg_2Si phase, likely due to small volume fraction as predicted by the Scheil simulations.

The following phases are not included in Fig. 15 or Table 5 and are only described for the sake of completeness as they are expected to form at temperatures above the processing temperatures of this study and/or may be present in relatively small amounts. For both the A356 and the A356 + Fe alloys, the CompuTherm simulations show that the $Ti_7Al_5Si_{14}$ and Al_3SiZr phases are expected to come out in the liquid at about 788 °C and 558 °C, respectively. The amount of these was found to be 0.27% and 0.009%, respectively, for both the BD and Scheil simulations. For the A356 + Fe alloy, the CompuTherm simulations show that the TiB_2, $Al_8Si_{15}Sr_4$, and $Al_{13}M_4$ phases are expected to come out in the liquid at about 1123, 656, and 623 °C, respectively. The amount of these was found to be 0.009, 0.028, and 0.019%, respectively, for both the BD and Scheil simulations.

Discussion

Comparison of ultrasonication processing with other grain refining technologies

Local ultrasonic processing was applied to two Al–Si–Mg alloys, A356 (0.09 wt.% Fe) and A356 + Fe (0.91 wt% Fe), to refine the as-cast microstructure of the alloys as they solidified. This process differs from

Table 5 Phases and their calculated amounts (%) using the Al material database (CompuTherm) and microstructure module in ProCAST for the as-cast condition

Alloy	Model	α-Al	Si (D-A4)	β-Al_5FeSi	$Al_8FeMg_3Si_6$	$Al_{15}FeMn_3Si_2$	Si_2V	Mg_2Si
A356	BD	94.2	5.20	0.29	0.06	–	0.02	–
	Scheil	93.8	5.23	0.27	0.11	–	0.01	0.32
A356 + Fe	BD	91.4	4.82	3.33	0.03	0.02	0.02	–
	Scheil	91.1	4.88	3.31	0.08	0.02	0.01	0.27

most other applications of ultrasonic melt processing in that ultrasound is applied to the melt as it solidifies in the mold, rather than applying ultrasound to the melt before it is poured or while it is being poured into a mold. The intent of the present approach was to ensure that the grain-refining effects of the ultrasound can be targeted to a specific local region of a shaped casting. For example, ultrasonic melt processing has historically been applied to wrought alloys during ingot casting to refine the bulk microstructure, resulting in increased plasticity and enabling large-scale ingots to be cast without hot cracking or other casting defects [8]. These ingots would then be forged into the final product form that showed better mechanical properties than if the ingot was not sonicated. Local ultrasonic processing presented in the current work, however, is expected to be applied to shaped castings (*e.g.*, automotive, aerospace, etc. applications). This means that in the final casting/component, the region of ultrasonic grain refinement will be localized to a specific location that has a different microstructure than the rest of the casting. For example, local ultrasonic processing could be incorporated into an existing permanent mold casting process to provide enhanced strength and ductility at a local region within the part where fatigue is a concern.

The application of local ultrasonic processing produced two non-dendritic microstructural morphologies in the primary Al grains: a globular morphology and a fine-grained morphology. The mean equivalent grain diameters of these microstructural morphologies, obtained by ultrasonically processing the alloys as they solidified, are smaller than the grain sizes that can be produced at similar cooling rates using conventional casting practices such as chills and grain refiners [2–5], and are similar to those of the non-dendritic microstructures produced using solid-state friction stir processing [6, 7]. However, local ultrasonic processing has the additional benefit of not requiring chemical modifiers (added to molten alloy) or additional post-casting processing steps (applied to the solidified alloy). Thus, local ultrasonic processing is expected to make components easier to sort and recycle, since the composition is not changed, and also help reduce the costs of implementing the technology, since the microstructure is refined during the casting process itself (*i.e.*, without adding another operation beyond casting).

Both the A356 and A356 + Fe ultrasonicated castings exhibited two non-dendritic microstructural morphologies for primary Al: a globular morphology and a fine-grained morphology. The globular microstructures in both the A356 and A356 + Fe ultrasonicated castings are similar to the microstructures reported in previous studies investigating ultrasonic melt processing [8, 9, 15, 19, 21]. To our knowledge, however, the fine-grained microstructural morphology has not been previously reported. Additionally, the previous studies investigating ultrasonic melt processing applied to A356 and 356 Al alloys studied alloys with Fe content only up to 0.66 wt. %, whereas this study investigated an alloy with almost 50% greater Fe content (0.91 wt.% Fe). This study also investigated two alloys with different Fe contents, whereas previous studies investigated only a single alloy. Our data shows that of the two alloys studied, local ultrasonic processing for microstructural modification is more effective in the A356 + Fe alloy as the size of the ultrasonically modified zone is over 20 times larger than in the A356 casting. The following section will discuss the effect of Fe on the size of the ultrasonically modified zone.

Formation of globular microstructure

Some of the primary Al grains observed throughout the globular microstructures have a rosette-like appearance, with short and round arms (see Fig. 6b and 7b). This morphology suggests that the application of ultrasound slowed the tip growth velocity of dendrite arms, as observed by Zhang et al. during *in-situ* tomography experiments with an Al-Cu alloy [15]. During steady-state solidification conditions, the tip of the dendrite grows into the hotter part of the melt. Because the solubility limit of Si in the α-Al phase is less than the Si content of the bulk alloy, Si is rejected laterally from the dendrite arms and becomes trapped in the inter-dendritic liquid, raising the local concentration of Si and thus lowering the local liquidus relative to near the tip of the dendrite arm. Sufficient mixing from ultrasound, however, would help homogenize the liquid, thus reducing any thermal and concentration gradients. This in turn would reduce the growth velocity at the tip of the dendrite arms relative to the thickening of the dendrite arms near the root, resulting in the observed rosette-like appearance.

While the globular microstructure, shown in Fig. 4b and 5b, was observed in both the A356 and A356 + Fe ultrasonicated castings, the distances at which the globular morphology was observed drastically varied.

For the A356 + Fe ultrasonicated casting, the globular microstructure was observed throughout the majority of the specimen and was observed at distances as far as 45 mm away from the location of the ultrasound probe. In the A356 ultrasonicated casting, however, the globular microstructural morphology is only observed at distances much closer to the ultrasound probe (≤ 6 mm). Repeat casting experiments replicated these same results and increasing the amplitude of the ultrasonic probe vibrations did not increase the distance at which the globular morphology was observed in the A356 alloy. The primary differences between A356 and A356 + Fe alloys are their compositions and solidification sequences. In the A356 alloy, the only solid phases between the liquidus and eutectic temperature are the primary Al phase (which is different from the eutectic Al phase, which begins to solidify at the eutectic temperature) and the Si_2V phase (of which there is less than 0.02%). In the A356 + Fe alloy, however, the β-Al_5FeSi phase begins to solidify at a temperature just below the liquidus, 608 °C. This means that in the A356 + Fe alloy, there is an additional solid phase present between 608 °C and 571 °C. The A356 + Fe casting has approximately 10 times as much Fe as the A356 alloy (0.91 wt.% compared to 0.09 wt.%, see Table 1), and is expected to have 11 to 12 times as much β-Al_5FeSi as the A356 alloy (see Table 5).

These data suggest that the greater amount of β-Al_5FeSi phase in the A356 + Fe alloy compared to the A356 alloy may have an effect on the size of the ultrasonically modified zone (*i.e.*, the total area of ultrasonically modified fine grains and globular grains). One possible explanation is that β-Al_5FeSi phase particles may serve as sites for cavitation bubbles to nucleate on, which in turn promote the nucleation of primary aluminum grains. Another possible explanation is that the presence of additional solid particles (*i.e.*, β-Al_5FeSi) along with primary Al grains being stirred within the semi-solid alloy may increase the probability of dendrites fragmenting. Another possible explanation is that, according to the thermodynamic simulation data, the A356 + Fe alloy has a slightly lower liquidus than the A356 alloy. While this temperature difference is only a few degrees Celsius, it may mean that the A356 + Fe alloy is fully liquid for a sufficiently long time to allow the ultrasound to propagate further into the liquid before any solid phases begin to form.

Additionally, in the A356 + Fe ultrasonicated casting, β-Al_5FeSi phase particles within ~ 5 mm of the ultrasound probe exhibited rectangular morphology, as opposed to the needle-shaped morphology of β-Al_5FeSi phase particles at distances further away from the ultrasound probe and in the A356 + Fe control casting. This difference in morphology suggests that the mechanism by which the β-Al_5FeSi phase grew at distance within ~ 5 mm of the ultrasound probe in the A356 + Fe ultrasonicated casting was different than at distances further away from the ultrasound probe or in the A356 control casting. During conventional solidification (without ultrasound), the β-Al_5FeSi phase grows anisotropically to accommodate the rapid movement of atoms across the solid–liquid interface, forming a metastable needle-like shape with high surface energy [31]. During extended heat treatments (~ 24 h), atoms are able to diffuse from the high-energy interfaces at the edges of the platelets to the low-energy interfaces at the faces of the plates [31]. This atomic diffusion produces a rectangular morphology similar in size and aspect ratio as the rectangular β-Al_5FeSi phase particles observed near the ultrasound probe in this study. This suggests that the growth of the rectangular morphology beta-phase particles at distances within 6 mm of the ultrasound probe is predominantly diffusion controlled unlike the growth of the needle-like beta-phase particles whose growth is predominantly interface controlled. This enhancement of diffusion-controlled growth could be a result of the enhanced mass transfer via ultrasonic mixing and/or higher thermal energy due to dissipation of ultrasonic energy as heat.

Another possible explanation for this rectangular morphology worth considering is enhanced nucleation, although, as described below, this mechanism is likely not operative here. In Al-Si cast alloys, the β-Al_5FeSi phase nucleates on the wetted exterior surfaces of oxide films [32]. These oxide films typically have two sides, one wetted and one dry. This dry, unbonded side can produce cracks in the β-Al_5FeSi phase if the film is folded over itself, or can give the appearance of "decohesion" between the β-Al_5FeSi phase and the matrix if the β-Al_5FeSi phase only nucleates on one side of the film [32]. Ultrasonic melt processing is known to increase the wettability of impurities in the melt [9–12]. It is possible that ultrasound may have increased the wettability of the oxide films on both sides of the film as well, thus increasing the number of potential sites for nucleation of the β-Al_5FeSi phase. However, this would likely increase the number and decrease the overall size of the β-Al_5FeSi particles rather than changing their morphology from needle-like to rectangular. Therefore, it is unlikely that enhanced nucleation via increased wettability of oxide films is responsible for the rectangular morphology of the β-Al_5FeSi particles near the ultrasound probe.

High Fe content in Al-Si alloys can make the alloy weaker and less ductile, particularly when the brittle and needle-shaped β-Al_5FeSi phase forms [25]. The needle-like morphology of the β-Al_5FeSi phase can act as a source of stress concentration within the alloy, which reduces the ductility and ultimate tensile strength of the alloy. A rectangular morphology, with lower aspect ratio than the needle shape, is expected to be a less severe source of stress concentration. Therefore, ultrasonic processing needs to be optimized to change the morphology of the beta-phase throughout the cross-section of a component, to potentially reduce the deleterious effects of the β-Al_5FeSi phase and further enhance the performance of high Fe alloys. This in turn could enable the greater use of recycle-grade high-Fe content Al alloys in applications where strength and ductility are a concern.

Formation of fine-grained microstructure

The fine-grained microstructures, shown in Fig. 4c and 5c, were only observed within 2 mm of the location of the ultrasound probe in both the A356 and A356 + Fe ultrasonicated castings. These microstructures have smaller Al grains than the globular morphology and relatively large, blocky Si and β-Al_5FeSi phase particles compared to the respective phases within the globular microstructure region. While the Ti from the ultrasound probe could potentially react with molten Al to from the Al_3Ti phase, which is an effective grain refiner in aluminum-based alloys, our experimental procedures avoided such a reaction. Furthermore, EDS and EBSD analysis did not detect any Ti-containing phases in the microstructure. In the fine-grained microstructures of both ultrasonicated castings, there is a local enrichment of Si particles, as the volume fraction of Si (15% and 17% in the A356 and A356 + Fe ultrasonicated castings, respectively) is twice that of their respective globular microstructures. In fact, the volume fraction of Si in the fine-grained microstructures is closer to the volume fraction of Si in unmodified Al-Si eutectic [30] than to the overall volume fraction of Si content in the alloy, 8%. This suggests that the fine-grained microstructure might be a large region consisting entirely of eutectic Al and eutectic Si grains with no primary Al grains (though the fine-grained microstructure of the A356 + Fe ultrasonicated casting may also contain primary Si grains, as described below). While the increased size of the Si particles may be deleterious to the ductility of the fine-grained microstructure, the presence of primary Si particles in the A356 + Fe fine grained microstructure and abundance of Si particles may increase local wear resistance.

The coarse and flakelike morphology of the Si particles in the as-cast A356 fine-grained microstructure (Fig. 8c) resembles the unmodified morphologies of Al-Si castings formed with slow cooling rates [30]. Furthermore, the granular appearance of Si in the as-cast A356 + Fe fine-grained microstructure (Fig. 9c) resembles the morphology of a divorced Al-Si eutectic, which is more commonly observed in hypereutectic Al-Si alloys that form with slow cooling rates [33]. Therefore, these Si morphologies suggest that the fine-grained microstructures in both ultrasonicated castings may have formed in regions where the local cooling rate was slower. Since the fine-grained region cools at a slower rate than the rest of the casting, it's solidification would be delayed compared to the rest of the casting. It is possible that as the surrounding regions solidified, the fine-grained region became more saturated with alloying elements (Si) before it cooled enough to begin solidification. Since the A356 alloy is hypoeutectic, as the primary Al grains form during solidification the surrounding liquid becomes supersaturated with alloying elements (Si) [30]. This increased concentration of Si would lower the liquidus in the local region, thus further delaying the onset of solidification and allowing the region to become further saturated, approaching the Al-Si eutectic composition. This sequence of events would then continue until the temperature of the local region reached the eutectic temperature, at which point the region would solidify as a eutectic.

In the A356 + Fe ultrasonicated casting, the above described sequence of events appears to have continued until the concentration of Si slightly exceeded the eutectic composition (as a Si area fraction of 17% is roughly equivalent to a mass fraction of 15 wt.%), making the fine-grained region of the A356 + Fe ultrasonicated casting hypereutectic and supercooled. As such, the pro-eutectic Si phase would begin to form at a temperature above the eutectic temperature. The abundance of the β-Al_5FeSi phase particles in the A356 + Fe casting could serve as nucleation sites for

Si particles. Thus, the two proposed requirements for divorced eutectic solidification, an abundance of fine Si particles in the melt before the eutectic reaction and a slow cooling rate across the temperature range of the eutectic reaction [33], would be fulfilled in the fine-grained region of the A356 + Fe ultrasonicated casting.

The slow cooling rate of the fine-grained region compared to the rest of the casting could be the result of dissipation of acoustic energy into heat, increased local pressure near the face of the ultrasound probe, or enhanced mixing. Computational fluid dynamics (CFD) simulations of ultrasound applied to molten Al by Riedel et al. measured a higher volume fraction of cavities near the face of a cylindrical ultrasound probe similar in geometry to the probe used in this study [34]. Additionally, Riedel et al. also tracked a high density of collapsed bubbles near the outer edge of the face of the probe [34], the same region where the fine-grained microstructure was observed in this work (Figs. 3 and 7). These collapsing bubbles would create a local region of high, oscillating pressure that could slow the cooling rate near the outer edge of the face of the ultrasound probe. Another possible reason for the fine-grained microstructure could be related to the side lobes [35] of the ultrasound probe. These side lobes form as a result of the probe's radial expansion and contraction that occurs simultaneously with the probe's longitudinal oscillations. These side lobes could have been reflected by the curved walls of the mold, producing a region of greater mixing in the immediate vicinity of the face of the probe and the mold wall. Together, these effects could possibly account for the unique, extremely fine Al grains that are 24% and 74% smaller, respectively, than the globular grains in the corresponding A356 and A356 + Fe ultrasonicated castings, which were observed at distances further away from the ultrasound probe.

Shape of ultrasonically-modified zone

In the present work, the ultrasonically-modified zone refers to the regions in the ultrasonically processed cast specimen that have a fine-grained or globular microstructural morphology. This ultrasonically-modified zone is surrounded by an unmodified dendritic morphology, which suggests that regions outside of the ultrasonically-modified zone solidified before they could be ultrasonically refined. CFD simulations by Riedel et al. showed that the shape of the acoustic streaming pattern in a large container of molten A356 is initially tear-drop shaped before recirculation [34]. The acoustic flow is expected to propagate normal to the face of the ultrasound probe and then recirculate back towards the ultrasound probe until the entire volume of liquid is mixed [34]. However, as the alloy solidifies, the viscosity of the semi-solid alloy increases and attenuation increases, which will affect the propagation of acoustic flow into the material and the size of the cavitation zone. In the A356 + Fe ultrasonicated casting, the shape of the ultrasonically-modified zone is tear-drop shaped (see Fig. 20), narrowing just in front of the probe and then widening at distances further away from the probe. This suggests that the alloy solidified too quickly for the acoustic stream to be fully established and fully mix the entire volume of material.

Conclusions

Local ultrasonic processing was applied to two A356 aluminum alloys, one with 0.09 wt.% Fe and one with 0.91 wt.% Fe, during solidification in a graphite mold. The resultant microstructures were observed to be significantly refined and were characterized by optical microscopy and SEM. Thermodynamic modeling was conducted to estimate the solidification ranges and phase fractions of each alloy. The following conclusions were reached:

1. The application of local ultrasonic processing produced two non-dendritic microstructural morphologies in the ultrasonically modified zone of the castings: (1) a globular microstructure and (2) a fine-grained microstructure (which has not been previously reported). In the A356 ultrasonicated casting, the primary aluminum grains of the globular and fine-grained microstructures are 89% and 91% smaller than the dendritic grains of the A356 control casting. In the A356 + Fe ultrasonicated casting, the primary aluminum grains of the globular and fine-grained microstructures are 74% and 93% smaller than the dendritic grains of the A356 + Fe control casting.
2. After T6 heat treatment, the Si particles in the globular microstructure of the A356 ultrasonicated casting are smaller and rounder (with 12% smaller equivalent diameter and 31% greater sphericity) than those of the A356 control casting. The Si particles in the globular microstructure of the A356 + Fe

ultrasonicated casting, however, are approximately equivalent in size and roundness (with 2% larger equivalent diameter and 5% greater sphericity) to those of the A356 + Fe control casting.

3. While the Al grains in the fine-grained microstructure region of the ultrasonicated castings are refined significantly, the Si particles are coarse relative to the Si particles in their respective control castings, even after a T6 heat treatment. The average equivalent diameter of the Si particles of the fine-grained microstructures of the A356 and A356 + Fe ultrasonicated castings are 31% larger and 102% larger, respectively, than their respective control castings. The large size and angular morphology of the Si particles in as-cast condition suggests that the region of the fine-grained microstructure cooled at a slower rate than the rest of the casting.
4. The fine-grained microstructure regions of both ultrasonicated castings appear to be large regions of fully Al-Si eutectic. In these regions, there in an enrichment of Si compared to their respective globular microstructures (with Si area fractions 2.3 and 2 times greater in the fine-grained regions of the A356 and A356 + Fe ultrasonicated castings, respectively, compared to the corresponding globular regions). This increased amount of Si may be a result of delayed solidification in the fine-grained region compared to the globular region, allowing the liquid in the fine-grained region to become more saturated with Si prior to solidification.
5. At distances less than 5 mm away from the ultrasound probe in the A356 + Fe ultrasonicated casting, the morphology of the β-Al_5FeSi particles in the fine-grained and globular microstructures changed from needle-like to rectangular (with aspect ratios 70% and 59% less, respectively, than the aspect ratio of the β-Al_5FeSi particles in the A356 + Fe control casting). This ultrasonically driven change in morphology and reduction in aspect ratio is expected to reduce the deleterious stress-concentration effects of the β-Al_5FeSi phase on the bulk strength of the alloy. Thus, the application of ultrasound is expected to further enhance the performance of high-Fe alloys, specifically near the source of ultrasound.
6. Despite being cast using the same conditions, the size of the ultrasonically modified zone in the A356 + Fe (high-Fe) ultrasonicated casting was 20 times larger than that of the A356 (low-Fe) ultrasonicated casting. This suggests that increased Fe content may enhance the ability of ultrasound to refine the microstructure.
7. The larger modified zone in the high-Fe alloy is hypothesized to be due to the β-Al_5FeSi phase serving as additional nucleation sites for the primary Al grains at temperatures just below the liquidus. These β-Al_5FeSi phase particles could also contribute to the fragmentation of dendrites. Thermodynamic modeling predicts the A356 + Fe alloy to have 11 to 12 times more β-Al_5FeSi phase than the A356 alloy. The β-Al_5FeSi phase is also predicted to form earlier in the A356 + Fe alloy at 608 °C (which is just below the liquidus temperature), whereas in the A356 alloy the β-Al_5FeSi phase begins to form at 571 °C (which is just below the eutectic temperature). Additionally, the liquidus of the A356 + Fe alloy is predicted to be at a slightly lower temperature than the A356 alloy, which would delay the onset of solidification and could allow for ultrasound to penetrate further into the casting, thus increasing the size of the ultrasonically modified zone.

Acknowledgements

The project was funded by the Department of Energy Vehicle Technologies Office as part of the Lightweight Metals Core Program. This research was conducted at PNNL, under Contract No. DE-AC05-76L01830 with the U.S. Department of Energy and UT-Battelle, LLC, under Contract No. DE-AC05-00OR22725 with the U.S. Department of Energy. The authors thank Mr. David Weiss at Eck Industries for providing the alloys for this work and technical discussions. The authors also thank Jens Darsell, Jon Helgeland, Anthony Guzman, Michael Blazon, and Nathan Canfield of Pacific Northwest National Laboratory for their technical assistance.

Authors contributions

K.E.R contributed to Data Curation, Formal Analysis, Investigation (Lead), Project Administration (Support), Visualization, Writing- Original Draft; A.S.S contributed to Investigation (Support), Writing- Review & Editing; A.R contributed to Conceptualization, Funding Acquisition, Project Administration (Lead), Supervision, Writing—Review & Editing.

Declarations

Conflict of interest The authors declare that a provisional patent (provisional application # 63/521,392) titled "Fabrication of Castings with Local Application of Ultrasound During Solidification" was filed on June 16, 2023 based on the casting work described in this manuscript.

Appendix

See Figs. 16, 17, 18, 19, 20

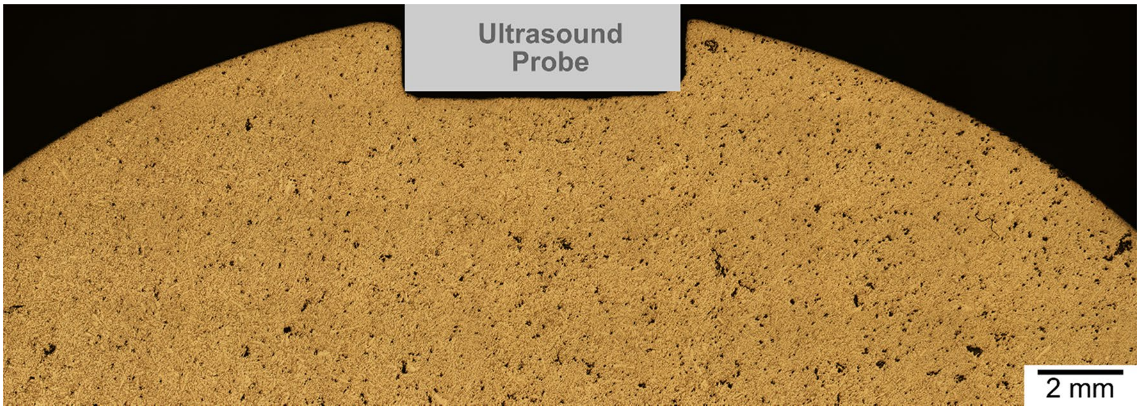

Figure 16 This image, stitched together from multiple optical micrographs, shows the dendritic microstructural morphology of the A356 control casting near the location of the ultrasound probe, which was inserted into the mold during casting but did not oscillate.

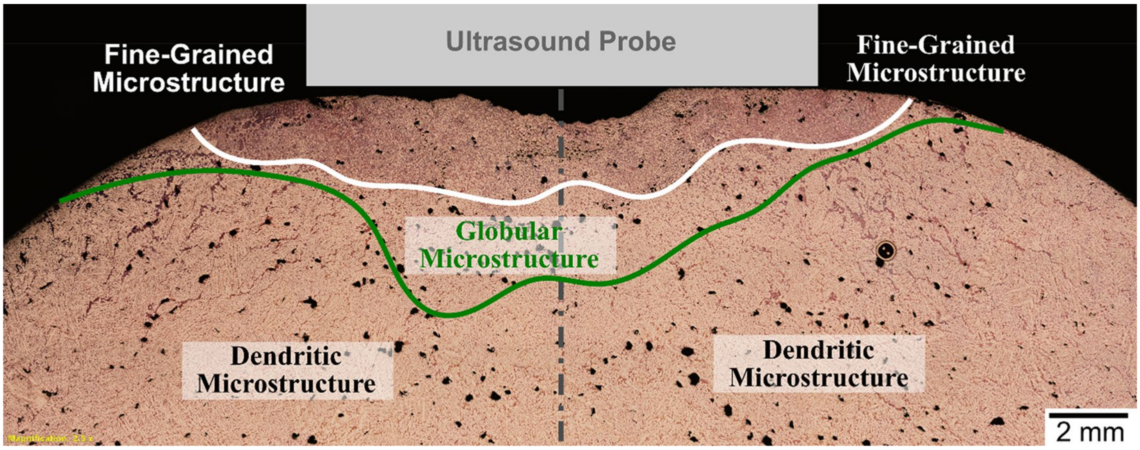

Figure 17 This image, stitched together fro multiple optical micrographs, shows the regions of each microstructural morphology in the A356 ultrasonicated casting relative to the ultrasound probe. The longitudinal axis of the ultrasound probe is identified with a dot-dashed line. For this casting, the amplitude setting of the ultrasound system was set at 33 μm.

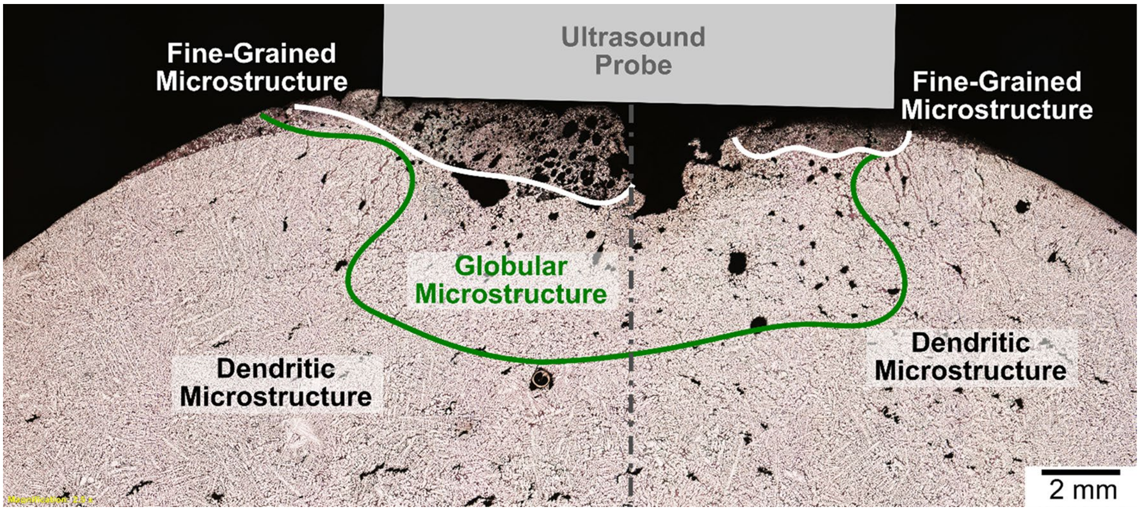

Figure 18 This image, stitched together from multiple optical micrographs, shows the regions of each microstructural morphology in an A356 alloy cast with ultrasound relative to the location of the ultrasound probe. For this casting, the amplitude setting of the ultrasound system was raised to 78 µm.

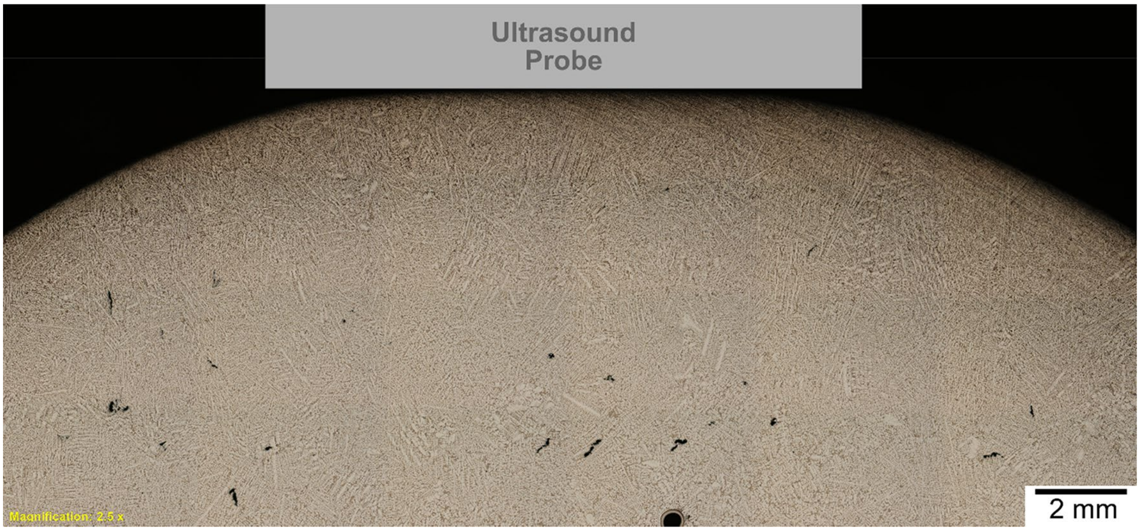

Figure 19 This image, stitched together from multiple optical micrographs, shows the dendritic microstructural morphology of the A356 + Fe control casting near the location of the ultrasound probe, which was inserted into the mold during casting but did not oscillate.

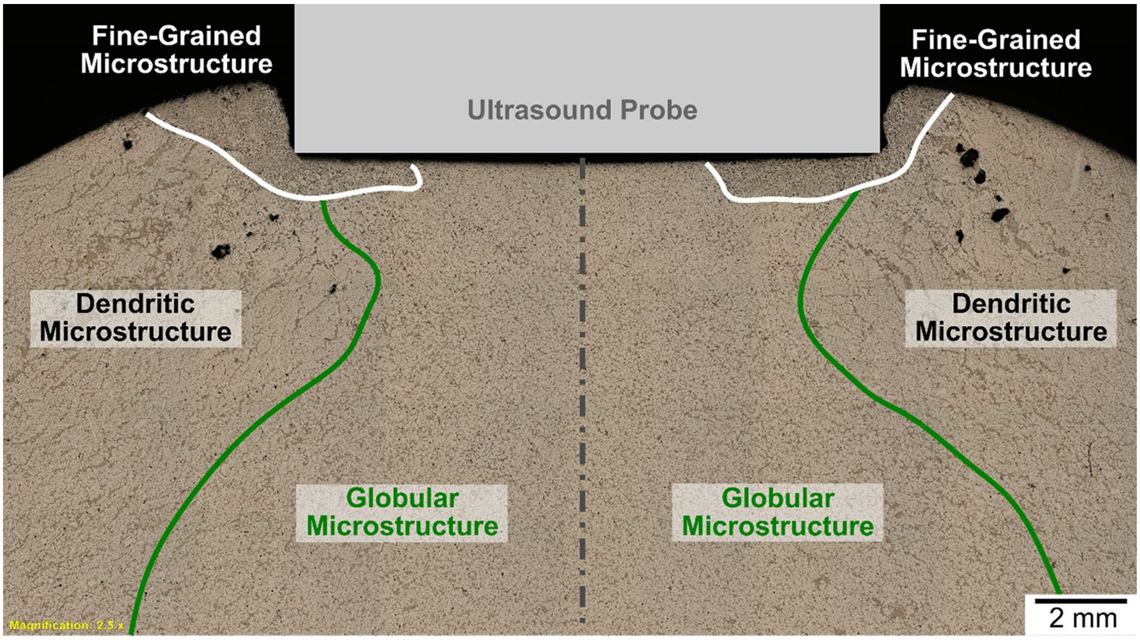

Figure 20 This image, stitched together from multiple optical micrographs, shows the regions of each microstructural morphology in the A356 + Fe ultrasonicated casting relative to the ultrasound probe. The longitudinal axis of the ultrasound probe is identified with a dot-dashed line. For this casting, the amplitude setting of the ultrasound system was set at 33 µm.

References

[1] Abraham A, Schultz R, Rakoto B, Murphy J, Ling L, Merta M, Dudley J (2020) 2020 North America Light Vehicle Aluminum Content and Outlook. Ducker Frontier. https://drivealuminum.org/resources/outlooks-and-ducker/

[2] Zhang LY, Jiang YH, Ma Z, Shan SF, Jia YZ, Fan CZ, Wang WK (2008) Effect of cooling rate on solidified microstructure and mechanical properties of aluminum- A356 alloy. J Mater Process Tech 207:107–111

[3] Sigworth GK, Kuhn TA (2007) Grain refinement of aluminum casting alloys. Int J Metalcast 1:31–40

[4] Yu L, Liu X, Wang Z, Bian X (2005) Grain refinement of A356 alloy by AlTiC/AlTiB master alloys. J Mater Sci 40:3865–3867

[5] Peeratatsuwan C, Chowwanonthapunya T (2020) Investigation on the grain refining performance of Al-5Ti-1B master alloy on the recycling process of A356 alloy. Materialwiss Werkstofftech 51:1346–1352

[6] Nelaturu P, Jana S, Mishra RS, Grant G, Carlson BE (2018) Influence of friction stir processing on the room temperature fatigue cracking mechanisms of A356 aluminum alloy. Mater Sci Engr A 716:165–178

[7] Ma ZY, Sharma SR, Mishra RS (2006) Microstructural modification of as-cast Al-Si-Mg alloy by friction stir processing. Met Mater Trans A 37:3323–3336

[8] Eskin GI (2001) Broad prospects for commercial application of the ultrasonic (cavitation) melt treatment of light alloys. Ultrasonics Sonochem 8:319–325

[9] Khalifa W, Tsunekawa Y, Okumiya M (2008) Effect of ultrasonic melt treatment on microstructure of A356 aluminum cast alloys. Int J Cast Metals Res 21(1–4):129–134

[10] Zhang L, Eskin DG, Katgerman L (2011) Influence of ultrasonic melt treatment on the formation of primary intermetallics and related grain refinement in aluminum alloys. J Mater Sci 26:5252–5259

[11] Kotadia HR, Qian M, Eskin DG, Das A (2017) On the microstructural refinement in commercial purity Al and Al-10 wt% Cu alloy under ultrasonication during solidification. Mater Des 132:266–274

[12] Jian X, Xu H, Meek TT, Han Q (2005) Effect of power ultrasound on solidification of aluminum A356 alloy. Mater Lett 59(2–3):190–193

[13] Eskin D (2014) Ultrasonic melt processing: Opportunities and misconceptions. Mater Sci Forum 794–796:101–106

[14] Shu D, Sun B, Mi JW, Grant PS (2012) A high-speed imaging and modeling study of dendrite fragmentation caused by ultrasonic cavitation. Metall and Mater Trans A 43A:3755–3766

[15] Zhang Z, Wang C, Koe B, Schleputz CM, Irvine S, Mi J (2021) Synchrotron X-ray imaging and ultrafast tomography in-situ study of the fragmentation and growth

dynamics of dendritic microstructure in solidification under ultrasound. Acta Mater 209(116796):1–12

[16] Huang H, Shu D, Fu Y, Wang J, Sun B (2014) Synchrotron radiation X-ray imaging of cavitation bubbles in Al-Cu alloy melt. Ultrason Sonochem 21:1275–1278

[17] Tzanakis I, Xu WW, Eskin DG, Lee PD, Kotsovinos N (2015) In situ observation and analysis of ultrasonic capillary effect in molten aluminum. Ultrason Sonochem 27:72–80

[18] Xu WW, Tzanakis I, Srirangam P, Mirihanage WU, Eskin DG, Bodey AJ, Lee PD (2016) Synchrotron quantification of ultrasound cavitation and bubble dynamics in Al-10Cu melts. Ultrason Sonochem 31:355–361

[19] Wang F, Eskin D, Mi J, Wang C, Koe B, King A, Reinhard C, Connolley T (2017) A synchrotron X-radiography study of the fragmentation and refinement of primary intermetallic particles in an Al-35Cu alloy induced by ultrasonic melt processing. Acta Mater 141:142–153

[20] Wang F, Tzanakis I, Eskin D, Mi J, Connolley T (2017) In situ observation of ultrasonic cavitation-induced fragmentation of the primary crystals formed in Al alloys. Ultrason Sonochem 39:66–76

[21] Puga H, Barbosa J, Costa S, Ribeiro S, Pinto AMP, Prokic M (2013) Influence of undirect ultrasonic vibration on the microstructure and mechanical behavior of Al-Si-Cu alloy. Mater Sci Engr A 560:589–595

[22] Rader KE, Darsell J, Helgeland J, Canfield N, Roosendaal T, Nickerson E, Denny A, Rohatgi A (2023) Improving the mechanical properties of cast aluminum through ultrasonication-induced microstructural refinement. In: Broek S (ed) Light Metals 2023, The Minerals, Metals, & Materials Series. Springer, New York, pp 422–428

[23] Zhang L, Gao J, Wiredu Damoah LN, Robertson DG (2012) Removal of iron from aluminum: a review. Miner Proc Extr Met Rev 33(2):99–157

[24] Lampman S (2018) Permanent mold casting of aluminum alloys. In: Anderson K, Weritz J, Kaufman JG (ed) ASM Handbook 2A: 209–231. https://doi.org/10.31399/asm.hb.v02a.a0006513

[25] 356.0 and A356.0: Al-Si-Mg high-strength casting alloys (2019). In: Anderson K, Weritz J, Kaufman JG (ed) ASM Handbook 2B: 548–552. https://doi.org/10.31399/asm.hb.v02b.a0006568

[26] Abramoffv MD, Magalhaes PJ, Ram SJ (2004) Image processing with image. J Biophoton Int 11(7):36–42

[27] Guo J, Samonds MT (2007) Alloy thermal physical property prediction coupled computational thermodynamics with back diffusion consideration. J Phase Equilib Diffus 28:58–63

[28] J. Guo and M. T. Samonds T. (2004) Property prediction with coupled macro-micromodeling and computational thermodynamics. Proc. of MCSP6, Taiwan: Kaohsiung, pp 157–164

[29] Sabau AS, Mirmiran S, Glaspie C, Li S, Apelian D, Shyam A, Haynes JA, Rodriguez AF (2018) Hot-tearing assessment of multicomponent non-grain refined Al-Cu alloys for permanent mold castings based on load measurements in a constrained mold. Metal and Mater Trans B 49:1267–1287

[30] Wakhlouf, M (2008) Solidification of Eutectic Alloys; Aluminum-Silicon. ASM Handbook

[31] Basak CB, Babu NH (2016) Morphological changes and segregation of β-Al9Fe2Si2 phase: A perspective from better recyclability of cast Al-Si alloys. Mater Des 108:277–288

[32] Cao X, Campbell J (2006) Morphology of β-Al5FeSi phase in Al-Si cast alloys. Mater Trans 47(5):1303–1312

[33] Liao H, Wu Y, Chen H, Qian L (2022) Divorced eutectic solidification in hypereutectic Al-Si alloys. Metall Mater Trans A 53A:2346–2350

[34] Riedel E, Liepe M, Scharf S (2020) Simulation of ultrasonic induced cavitation and acoustic streaming in liquid and solidifying aluminum. Metals 10(47):1–22

[35] Quien MM, Saric M (2018) Ultrasound imaging artifacts: How to recognize them and how to avoid them. Echocardiography 35:1388–1401